

Temporal solitons and pulse compression in photonic crystal waveguides

P. Colman^{1,3†}, C. Husko^{1,2†}, S. Combré^{1†}, I. Sagnes³, C. W. Wong^{2*} and A. De Rossi^{1*}

Solitons are nonlinear waves that exhibit invariant or recurrent behaviour as they propagate. Precise control of dispersion and nonlinear effects governs soliton propagation and, through the formation of higher-order solitons, permits pulse compression. In recent years the development of photonic crystals—highly dispersive periodic dielectric media—has attracted a great deal of attention due to the facility to engineer and enhance both their nonlinear and dispersive effects. In this Article, we demonstrate the first experimental observations of optical solitons and pulse compression in ~1-mm-long photonic crystal waveguides. Suppression of two-photon absorption in the GaInP material is crucial to these observations. Compression of 3-ps pulses to a minimum duration of 580 fs with a simultaneously low pulse energy of ~20 pJ is achieved. These small-footprint devices open up the possibility of transferring soliton applications into integrated photonic chips.

Soliton propagation is a fascinating and ubiquitous property of nonlinear waves¹. In optics, temporal solitons² and pulse compression³ have been experimentally demonstrated in fibres, fibre Bragg gratings (FBGs)⁴ and photonic crystal fibres (PhCF)^{5–7}. Practical interest in solitons stems from the possibility of modifying and controlling the pulse shape (for example, compression) all-optically. Ultrafast compression has been reported previously in glass waveguides at wavelengths of 800 nm and with pulse energies of ~100 pJ or more^{8,9}. In silicon waveguides, optical solitons have also been observed spectrally^{10–12} with femtosecond input pulses. Much lower values for the excitation power of solitary waves have been demonstrated in systems with resonant nonlinearity, particularly self-induced transparency in helium-cooled doped fibres¹³. However, the available bandwidth is much smaller due to the resonant nature of the nonlinearity, and there are also issues in integrating such a device. The quest to demonstrate soliton dynamics at the chip scale is challenging due to the short (millimetre or less) interaction length and compatibility of compact laser sources (semiconductor laser diodes have pulse durations and energies limited to picoseconds and picojoules, respectively¹⁴), the combination of which has hindered the development of an integrable soliton compressor. Here, we experimentally demonstrate optical soliton compression in this unexplored regime of picosecond, picojoule pulses in a semiconductor chip.

Periodic dielectric structures have long been known to demonstrate extremely large dispersion, thereby enabling the observation of soliton effects at centimetre (or shorter) length scales^{4,15–18}. The reduced interaction length, however, requires a correspondingly larger intensity-dependent index modulation to match the strength of the dispersion. Increasing the optical intensity inside the waveguide is accomplished by inputting larger peak powers or decreasing the effective modal area^{8,10–12}. Recent progress in photonic crystal (PhC) technology has revealed another route using the potential for dispersion engineering and the related enhancement of the nonlinear response due to the slow-light effect^{19,20}, thus decreasing the threshold of nonlinear effects such as Kerr, multiphoton absorption or Raman

scattering^{21–23}. In addition to the aforementioned dispersion engineering, other research has focused on reducing the required intensity of chip-scale nonlinear effects by means of materials engineering. Semiconductors^{20,24}, chalcogenides^{25–28}, tellurites²⁹ and doped silica³⁰ have Kerr coefficients that are typically up to three orders of magnitude larger than that of silica fibre. The highly confined optical modes in dispersion-engineered semiconductor photonic crystal waveguides (PhCWGs) thus constitute a long-awaited development in low-intensity threshold nonlinearities to complement the well-established large dispersion of periodic media^{15–17,31–34}, facilitating this observation of soliton dynamics in PhCWGs.

A new parameter space for soliton physics

The present research was performed using a GaInP PhC membrane with a hexagonal lattice constant a of 485 nm, a hole radius of $0.20a$ and a thickness of 170 nm, with an added line defect of dielectric (termed a photonic crystal waveguide^{19,35}), as shown in the inset of Fig. 1a. The dispersion was tuned by increasing the innermost hole radii to $0.22a$. The 1.3-mm PhC waveguide included integrated mode adapters³⁶ to reduce the total input–output insertion losses to ~8 dB and suppress facet Fabry–Pérot oscillations. The propagation loss α , measured at a wavelength of $\lambda = 1,544$ nm, where $\alpha = 1$ dB mm⁻¹ at a group index of $n_g = 6$, approximately follows n_g^2 scaling^{37,38}. The waveguide dispersion properties are measured using the phase-shift method³⁷ (see Methods). Figure 1a shows the group index n_g increasing from 5 to ~13 in the range of interest. The group-velocity dispersion (GVD) coefficient, β_2 , and third-order dispersion (TOD) coefficient, β_3 , are also shown (Fig. 1b). The GVD is negative (anomalous) and on the order of ~ps² mm⁻¹, about five orders of magnitude larger than for silica fibre across the range of interest.

The nonlinear and dispersive effects of the optical solitons are captured by two length scales³⁹, a nonlinear length $L_{NL} (= 1/\gamma_{eff}P_0)$, where the effective nonlinear parameter γ_{eff} is given by $(n_2\omega_0/cA_{eff}) \cdot (n_g/n_0)^2$ (ref. 40) and P_0 is the pulse peak power, and a dispersion length $L_d (= T_0^2/|\beta_2|)$, where $T_0 = T/F$, T_{FWHM} is the

¹Thales Research and Technology, Route Départementale 128, 91767 Palaiseau, France, ²Optical Nanostructures Laboratory, Center for Integrated Science and Engineering, Solid-State Science and Engineering, and Mechanical Engineering, Columbia University, New York, New York 10027, USA,

³Laboratoire de Photonique et de Nanostructures (CNRS UPR 20), Route de Nozay, 91460 Marcoussis, France; [†]These authors contributed equally to this work. *e-mail: alfredo.derossi@thalesgroup.com; cww2104@columbia.edu

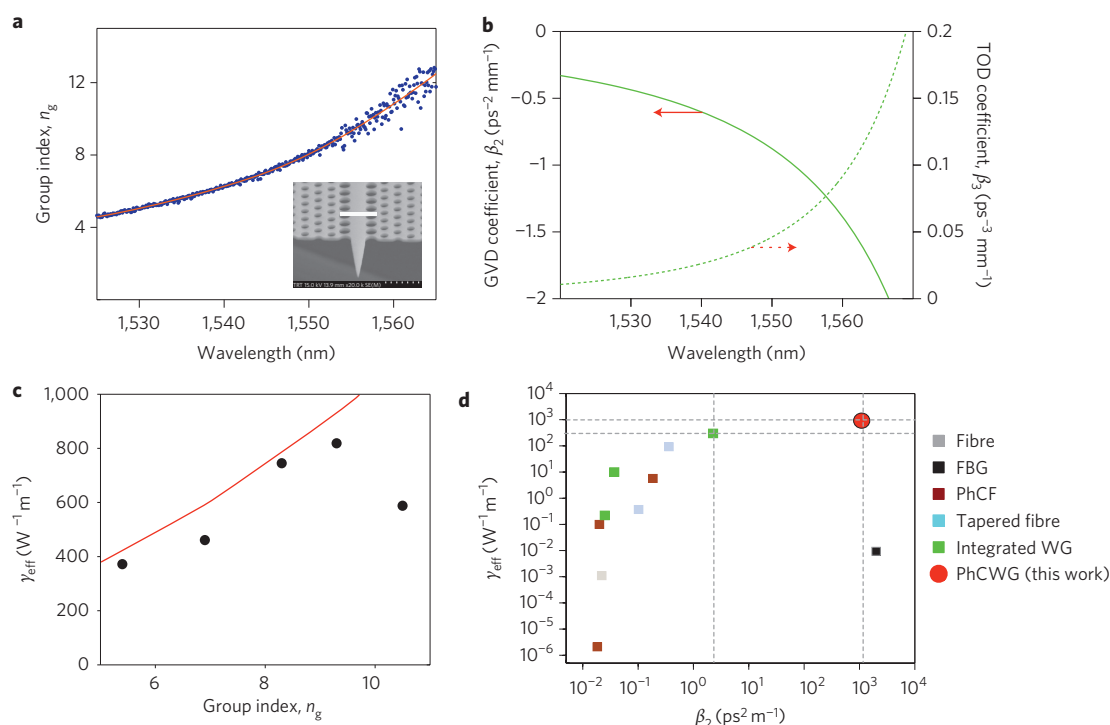


Figure 1 | Dispersion and slow-light properties of the GaInP PhCWG sample. **a**, Measured group index (dots) and fit (solid line)⁵⁰. Inset: scanning electron micrograph of a GaInP membrane with designed mode adapters³⁶ (scale bar, 1 μm). **b**, GVD coefficient (left axis) and TOD coefficient (right axis) derived from phase-shift group index measurements⁵⁰. At 1,551 nm, the GVD coefficient is $-0.91 \text{ ps}^2 \text{ mm}^{-1}$. **c**, Nonlinear parameter γ_{eff} extracted from experimental (dots) and theoretical (line) scaling^{19,21} due to slow-light enhancement. **d**, Nonlinear (γ_{eff}) and GVD (β_2) parameters of different material systems with experimentally demonstrated soliton effects. The PhCWG examined in this work simultaneously exhibits both large γ_{eff} and GVD coefficient in a single material system, together with suppressed two-photon absorption, enabling compression of picosecond pulses at picojoule energies (watt peak powers) and millimetre length scales. Inset in **a** is © 2009 AIP.

Table 1 | Material parameters of different material systems with experimentally demonstrated soliton effects.

System	β_2 ($\text{ps}^2 \text{ m}^{-1}$)	γ_{eff} ($\text{W}^{-1} \text{ m}^{-1}$)	E_c (pJ)	T_{FWHM} (ps)	Ref.
Fibre	0.022	0.0011	8	7	3
Fibre Bragg grating	2000	0.0094	1×10^6	80	4
Hollow PhCF	0.0183	0.000002	9×10^5	0.11	5
Nonlinear PhCF	0.02	0.10	25.4	0.041	9
Tellurite PhCF	0.185	5.70	573	0.40	29
Tapered PhCF fibre	0.10	0.37	500	0.07	8
Chalcogenide tapered fibre	0.36	93	2.2	0.25	25
Silica nanowire	0.009	0.22	71	0.60	30
Silicon nanowire	2.26	300	0.52	0.11	10–12
Chalcogenide nanowire	0.037	10	41.5	0.61	26
GaInP PhCWG (this work)	1100	920	12	3.25	

The key parameters in soliton formation, GVD coefficient β_2 and effective nonlinearity γ_{eff} , are tabulated. The experimental pulse conditions, pulse energy and duration applied in the experiments are also noted.

pulse width (full-width at half-maximum, FWHM) and $\Gamma = 2\sinh^{-1}(\sqrt{2}) = 1.76$. For 3-ps pulsewidths, L_d ranges from 6 mm to 1.6 mm. The nonlinear Kerr parameter γ_{eff} is inferred from the spectral broadening dependence on pulse peak power²³. The measured effective nonlinear parameter γ_{eff} is strongly dependent on n_g (Fig. 1c), with the largest value being just above $900 \text{ W}^{-1} \text{ m}^{-1}$ at 1,555 nm ($n_g = 9.3$). At larger group indices ($n_g > 10$), disorder-induced scattering⁴¹ and three-photon absorption²³ limit the effective Kerr nonlinearity, and the measured γ_{eff} parameter deviates from theoretical values. The 1.9-eV bandgap of GaInP completely suppresses two-photon absorption ($2h\nu = 1.6 \text{ eV}$ at 1,550 nm) such that residual band-tail absorption is negligible, as detailed in our recent studies⁴².

From fibres to integrated structures, Fig. 1d and Table 1 show the γ_{eff} and β_2 parameters of various systems in which soliton effects have been observed. The observed γ_{eff} in the present system is of the same

order of magnitude as that of integrated nanowires, being just slightly larger^{10–12}. The GVD coefficient for the present system is only a factor of two smaller than that of FBGs⁴. However, the semiconductor nanowires have a GVD coefficient that is a factor of $\sim 10^2$ smaller than the present set-up, and the FBGs have a γ_{eff} that is $\sim 10^5$ smaller in magnitude, consequently requiring much larger input powers (on the scale of kilowatts). In contrast with the present work, which makes use of approximately watt-level peak power and picosecond pulses, many of these demonstrations use femtosecond pulses, which markedly reduces the dispersion length.

Temporal soliton-effect pulse compression measurements

We next examined the output pulses directly in the time domain through second-harmonic intensity autocorrelation. Figure 2a,c shows a series of traces at 1,551 nm ($n_g = 8.3$) and 1,555 nm

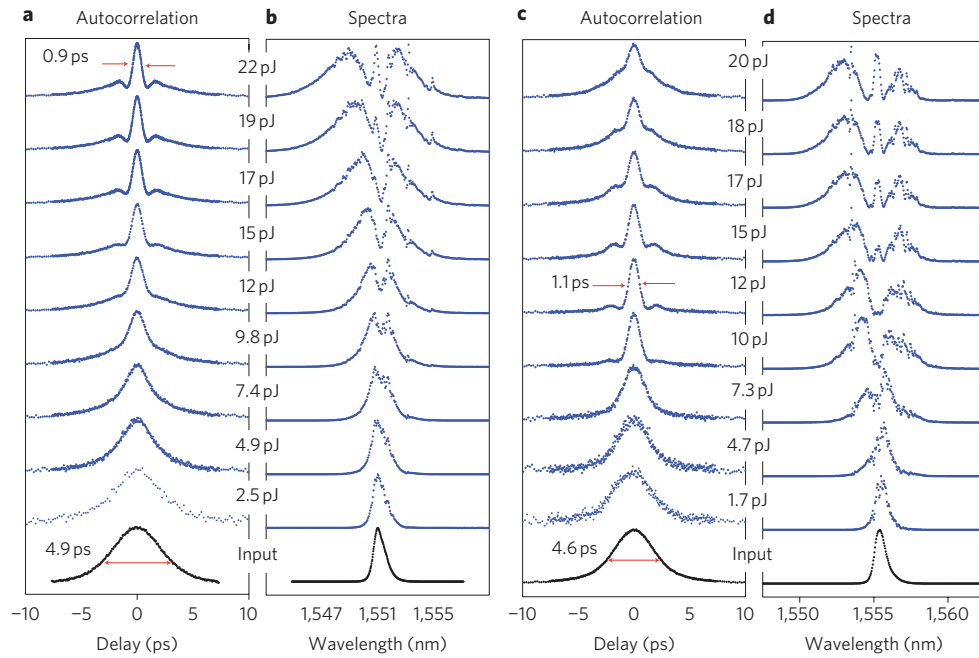


Figure 2 | Soliton-based pulse compression at coupled pulse energies of 22 pJ or less in 1.3-mm-long PhCWGs. **a–d**, Experimental intensity autocorrelation traces (**a,c**) of output pulses for increasing coupled pulse energies from 1.7 pJ to 22 pJ and corresponding spectra (**b,d**). Mode-locked pulses centred at 1,551 nm (**a,b**; $n_g = 8.3$). A minimum pulse width of 580 fs (sech² deconvolved; factor, 1.54) is achieved. Input pulse traces are also shown in black. Mode-locked pulses centred at 1,555 nm (**c,d**; $n_g = 9.3$). A minimum pulse width of 700 fs is achieved. Owing to the strong $\chi^{(3)}$ nonlinearity and wavelength-scale confinement, a minimum energy of 12 pJ enables 700 fs compression on a 1.3-mm length scale.

($n_g = 9.3$), respectively, for increasing coupled pulse energies, E_c (see Methods). The autocorrelation trace widths (FWHM) decrease from an input duration of 4.9 ps to a minimum of 900 fs at 22 pJ, for a compression ratio $\chi_c (=T_0/T_{\text{comp}})$ of 5.4. Applying an autocorrelation deconvolution factor of 1.54 for hyperbolic secant pulses suggests a pulse width compression from 3.2 ps to 580 fs. The measurements at 1,555 nm report a slightly broader minimum pulse width (1.1 ps from autocorrelation; 700 fs deconvolved). Note that the minimum width occurs at a pulse energy of 12 pJ, about one-half the energy compared to that measured at 1,551 nm due to the significantly larger nonlinear parameter γ_{eff} . Above 15 pJ, the autocorrelation trace deviates considerably from a bell shape; consequently, using the autocorrelation FWHM as a measure of pulse duration is not appropriate and these few points are not included in the quantitative analysis that follows. The associated spectral properties, increased spectral broadening with coupled pulse energy due to self-phase modulation (SPM), are shown in Fig. 2b,d.

Figure 3a shows the measured pulse width for the range of coupled pulse energies and group velocities examined. We identified three distinct regimes: (i) negligible pulse width change with pulse energy at 1,544 nm (with $n_g = 6.9$); (ii) pulse width decreases with energy monotonically down to 600 fs at 1,551 nm (with $n_g = 8.3$); and (iii) minimum pulse width (700 fs) achieved for an optimal value of the pulse energy at 1,555 nm (with $n_g = 9.3$). Soliton excitation, a regime in which the SPM-induced phase distortion exactly compensates for GVD, occurs when the pulse energy W is matched to the fundamental soliton energy W_0 , where $W_0 = 3.1\beta_2/(\gamma_{\text{eff}}T_{\text{FWHM}})$. At larger input energies, the formation of higher-order solitons characterized by the soliton number N (where $N^2 = W/W_0$) leads to notably different pulse evolution. In particular, the higher-order solitons undergo periodic modulation with soliton period $z_0 = \pi L_d/2$, as well as temporal pulse compression. In addition, larger N numbers lead to greater compression and evolve on shorter length scales^{39,43}. For a given N , an optimal

distance z_{opt} therefore exists at which the pulse experiences a minimum width. In our system, W_0 is 0.9 pJ (1,544 nm), 1.1 pJ (1,551 nm), 1.3 pJ (1,555 nm) and 1.4 pJ (1,559 nm). In this sample solitons with order N up to 4 (thus 16 times more energy than required to sustain a fundamental order soliton) are launched into the waveguide for compression.

The time–bandwidth product of the compressed pulses is presented in Fig. 3b. At 1,544 nm the product is initially close to 0.35, a near-ideal hyperbolic secant, and increases monotonically with input energy due to nonlinear pulse broadening and relatively weak dispersion. Interestingly, at 1,551 nm, the experimentally observed time–bandwidth product remains between 0.30 and 0.36, close to the 0.315 limit for hyperbolic secant pulses, and maintains this limit throughout the range of coupled energies. Our model (solid line), detailed below, reproduces this behaviour with quantitative agreement. The time–bandwidth product remains almost constant, because the input pulse is compressed adiabatically, without introducing additional chirp. This is the essence of soliton compression. The 1,555 nm curve follows a similar trend, which begins to increase above 15 pJ due to deviation from the optimal z_{opt} .

Figure 3c shows the estimated soliton number N of the output pulse versus the input value. The 1,544 nm measurements greatly contrast with the 1,551 nm case, where the value of N remains largely unchanged due to the significantly weaker nonlinear and dispersion effects. It is worth pointing out that the decrease in pulse temporal duration is the primary reason for the change in N , not loss. Linear and nonlinear losses also play a role, with either effect having a greater contribution depending on the input pulse energy. The soliton-effect pulse compression mechanism itself also redistributes a small amount of energy out of the central peak, ~ 1 dB for the soliton orders examined here^{39,43}. The total loss at the largest input energies and elevated group indices (for example, 1,551 nm for the 22 pJ pulse) is estimated to be 4.4 dB, with ~ 1.4 dB arising from linear loss, ~ 2 dB from nonlinear loss

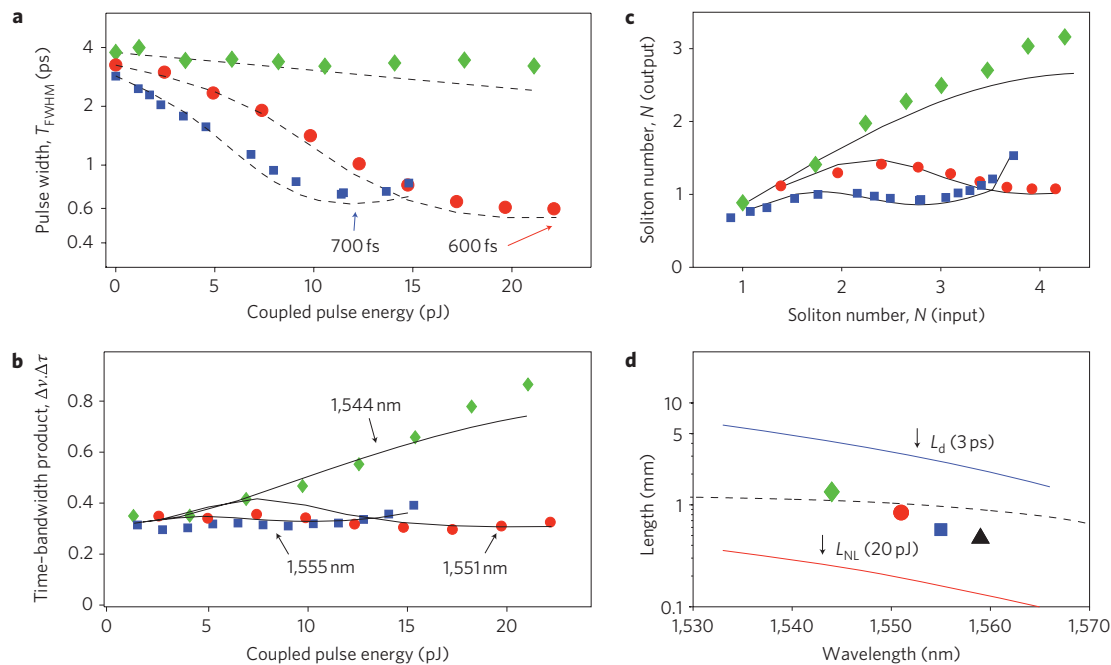


Figure 3 | Measurements demonstrating optical soliton compression. **a**, Measured (symbols) pulse widths after autocorrelation deconvolution versus the coupled pulse energy, at 1,544 nm ($n_g = 6.9$, diamonds), 1,551 nm ($n_g = 8.4$, dots) and 1,555 nm ($n_g = 9.3$, squares), respectively. Dashed lines are numerical results from the nonlinear Schrödinger model. **b**, Time-bandwidth product. Temporal pulse width is constant in the case of $\lambda = 1,544$ nm, consistent with $L_d \gg L$; however, bandwidth increases. Soliton compression with near-constant time-bandwidth product is observed at 1,551 nm. At the slow group velocities at 1,555 nm and 1,559 nm (not plotted), this regime breaks down at energies greater than ~ 17 pJ, where nonlinear absorption becomes important and removes energy from the optical soliton. **c**, Soliton number N at the output versus N at the input. **d**, Dispersion lengths L_d (~ 3 ps pulses) and nonlinear lengths L_{NL} (input energy, 20 pJ). The dashed curve is the effective length L_{eff} . The filled points are the optimal sample length, z_{opt} , for an input energy of 20 pJ. The measurements at 1,559 nm (triangles) are not plotted in panels **a-c**.

and 1 dB from compression. Additional improvements are possible for structures with optimized dispersion and improved level of fabrication.

To gain further insight into the interaction of various effects, we calculated the characteristic length scales, the effective length L_{eff} (dashed black line in Fig. 3d), the dispersion length L_d (blue line) and the nonlinear length L_{NL} (red line) at $\tau_p = 3$ ps and $E_c = 20$ pJ, at the various group indices examined in Fig. 3d. We also determined the optimal sample lengths z_{opt} at which to observe ideal compression for these parameters. At 1,544 nm ($n_g = 6.9$), z_{opt} is 1.7 mm, significantly longer than L_{eff} (1.1 mm; $z_{opt} > L_{eff}$), and the conditions for compression are not met. With the pulse centred at 1,551 nm, $z_{opt} \approx L_{eff} = 1.0$ mm, which accounts for the near-ideal compression observed in the measurements. At 1,555 nm, $z_{opt} = 0.61$ mm and $L_{eff} = 0.97$ mm, indicating that the pulse achieves its minimum width before exiting the waveguide. As a consequence, the pulse width at the output increases when further increasing the coupled pulse energy. We also consider the complementary metric of calculating the optimal coupling energy E_c so that $z_{opt} = L_{eff}$. Although the optimal energy required for 1,544 nm (26 pJ) was unreachable with our current set-up, both 1,551 nm (16 pJ) and 1,555 nm (10 pJ) were well within range. The autocorrelation data of Fig. 2c confirm that optimal narrowing is in fact achieved at ~ 12 pJ at 1,555 nm.

Nonlinear Schrödinger equation (NLSE) model

In the experimental conditions considered here, the PhC waveguide is operated far from the band edge, so the propagation of optical pulses is modelled using the nonlinear Schrödinger equation (NLSE) with a correction for slow light⁴⁰. This contrasts with the process for gap solitons, which are approximately described as a superposition of Bloch modes at the band edge^{18,31-33,44}, a regime

not achievable here due to the large level of backscattering⁴¹. The NLSE model is described by⁴⁰

$$\frac{\partial E}{\partial z} = -\frac{1}{v_g} \frac{\partial E}{\partial t} - i \frac{\beta_2}{2} \frac{\partial^2 E}{\partial t^2} + \frac{\beta_3}{6} \frac{\partial^3 E}{\partial t^3} - \frac{\alpha_1}{2} E + i \gamma_{eff} |E|^2 E - \frac{\alpha_{3eff}}{2} |E|^4 E + \left(ik_0 \delta - \frac{\sigma}{2} \right) N_c E \tag{1}$$

This includes TOD coefficient β_3 , group velocity v_g , linear propagation loss α_1 , effective slow-light three-photon nonlinear absorption α_{3eff} (ref. 23) and the effective nonlinear parameter γ_{eff} . We also included carrier effects through the generated carrier density N_c , the associated free-carrier dispersion δ and absorption σ . The auxiliary equation for the carrier density and the other parameters are given in the Supplementary Information. TOD coefficient, included in the model, contributes negligibly throughout the range of parameters examined here, even with minimum pulse durations. The nearly symmetrical spectra indicate that free-carrier effects play only a minor role, except at the largest pulse energies and group indices. We calculated the pulse temporal width (Fig. 4a,b) and output spectra (the latter not shown here) as a function of the coupled pulse energy. Importantly, the model leads to simultaneous agreement with both the autocorrelation and spectra with no degrees of freedom.

Interestingly, the centre peak of the pulse overlaps well with a hyperbolic secant and carries a substantial amount of the total pulse energy (56%). In the insets of Fig. 4a,b are also listed the compression factor $\chi_c = T_0/T_{comp}$ and the compression quality factor $Q_c = P_{peak}/\chi_c$, where P_{peak} is the output peak intensity normalized to the input peak intensity³⁹, measured experimentally and confirmed by numerical simulation. The procedure is repeated for the

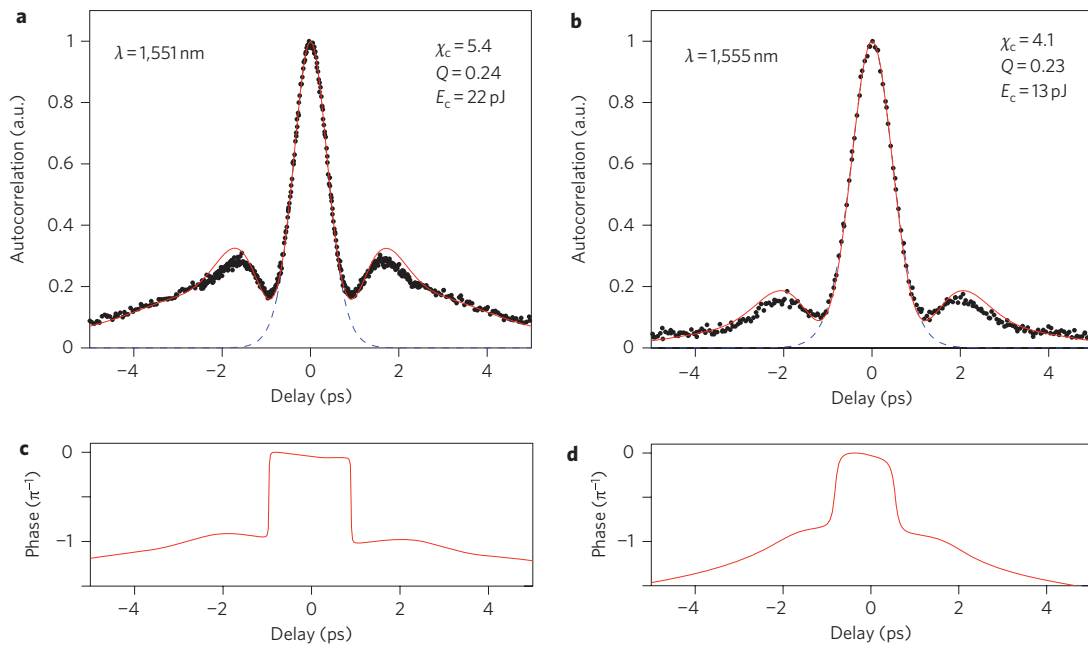


Figure 4 | Comparison of nonlinear Schrödinger equation model with experimental data. **a, b**, Measured autocorrelation traces (black dots) at 1,551 nm with a coupled pulse energy of 22 pJ (**a**), and at 1,555 nm with a coupled pulse energy of 13 pJ (**b**), together with the corresponding calculated autocorrelation traces (red solid line) and fit with a hyperbolic secant (blue dashed line). The experimental compression factor χ_c and quality factor Q_c are shown in the insets. **c, d**, The calculated phase is flat, indicating the balance of SPM and GVD, for example, the formation of an optical soliton.

shortest pulse at 1,555 nm and a value of 720 fs is retrieved (76% pulse energy in the centre peak). The quality factors here are restricted by three-photon absorption, which caps the maximum peak power. This point is discussed further below and in the Supplementary Information. Figure 4c,d shows plots of the pulse optical phase φ , which is flat across the main peak for the two cases at 1,551 nm and 1,555 nm. This corresponds to a balance of SPM and GVD at the output, and further strengthens the conclusion that the main peak is indeed a soliton. Full numerical simulations for the measurements in Fig. 2 are provided in the Supplementary Information.

The main impact of the dissipative terms in the NLSE is to slow down the soliton dynamics, for example, to increase the effective spatial scale. The ultimate limits to the system are twofold. The linear attenuation due to disorder-induced backscattering ultimately eliminates the periodic property of higher-order solitons. Regarding nonlinear absorption, three-photon absorption places a fundamental limit on the peak powers that can be produced, and thus forms an upper bound to the maximum compression achievable. Note that materials limited by two-photon absorption require much smaller critical intensities to trigger free-carrier effects. Two-photon-limited materials consequently experience larger attenuation and carrier dispersion, thus imposing even greater limitations on the compression mechanism, compared to three-photon-limited materials²⁰. Semiconductor material systems also differ from glass fibres, where the dominant effect at larger intensities is intrapulse Raman scattering³⁹.

For an anomalous dispersion waveguide with positive chirp, it is possible that temporal compression could be observed in the initial lengths of the waveguide without SPM or soliton formation. We experimentally verified that this effect is negligible using a number of methods. First, as the input pulses are nearly transform-limited, pre-input chirp is very small. Second, at low power (<1 pJ), we observed that the output pulse width is identical (within measurement error) to the input pulse. Third, the compression is directly related to the increase in the coupled energy, controlled with a fibre attenuator, such that the input pulse shape

remains unmodified throughout the experiment. In addition, note that the Raman contribution and related self-frequency shift^{11,45} are negligible, at our power levels, for this material, as seen in the pulse spectra measurements. Further increase of the compression factor relies on suppression of three-photon absorption with improved materials and nanofabrication, together with an examination of dispersion-managed PhCWGs for chirped or flat dispersion at low group velocities^{19,20}.

Demonstration of the soliton propagation regime

To further explore the soliton regime we conducted additional measurements with shorter pulses, so that the dispersion length was shorter than the device length, L (see Methods). Importantly, we input asymmetric pulses with an FWHM duration of ~ 1.8 ps and a spectral width of ~ 1.2 nm centred at 1,555 nm, giving a shortened dispersion length L_d of ~ 1.1 mm (compared with 2.82 mm in the previous experiment). Under these conditions ($L > L_d$), we observed dispersion-induced broadening at the lowest pulse energies (weak nonlinear effects; Fig. 5a). As the pulse energy was increased, the output pulse returned to the input duration before further compressing to a minimum duration of 800 fs (Fig. 5b), limited only by the output power of the laser. Despite the almost triangular autocorrelation input trace (significantly different from a hyperbolic secant input), the output pulse is very similar to that previously obtained with a different pulse shape but comparable energy. The ability of a pulse to redistribute its energy into a hyperbolic secant form is an important property of solitons.

We also checked for the potential degradation of noise due to soliton dynamics in the PhC. Using the Von der Linde method, we compared the radiofrequency spectra with 10 Hz resolution as a function of the harmonic order of the laser alone, and after the sample. We observed no discernable difference in the electrical spectra in terms of the ratio between the integrated noise pedestal and the signal spectral peak for several harmonics up to $n = 150$, within measurement accuracy.

We will finally comment on the potential impact of these devices in the scope of integrated optics. Recent developments in integrated

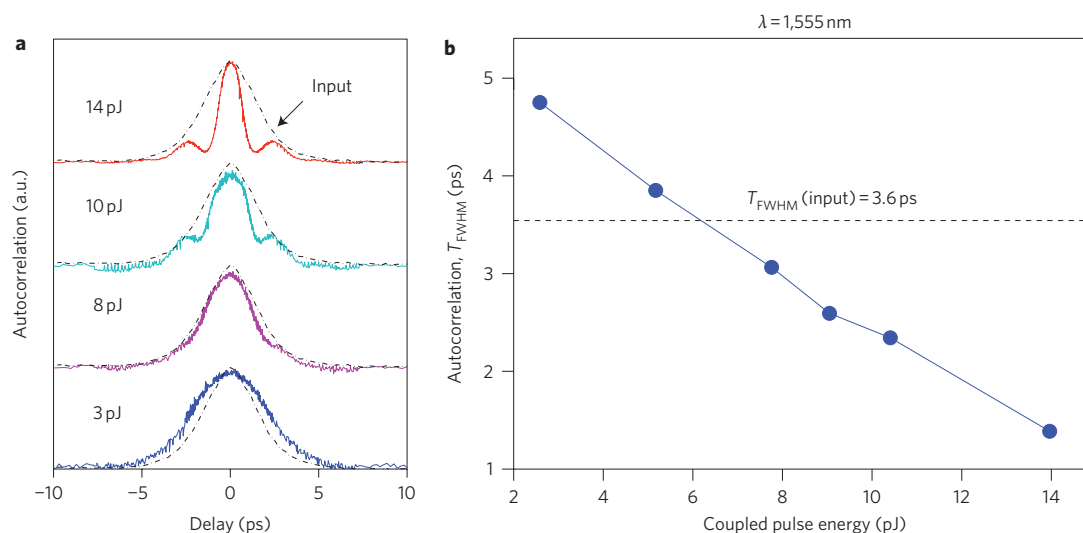


Figure 5 | Measurements demonstrating optical soliton formation. **a**, Autocorrelation measurements at 1,555 nm with 1.8-ps exponential input pulses (dotted lines). The autocorrelation trace is different from that of a sech^2 pulse. The pulse experiences dispersion-induced broadening at small pulse energies before contracting at larger pulse energies, thereby demonstrating soliton behaviour. **b**, As in Fig. 3a at 1,555 nm, but with 1.8-ps exponential pulses. The pulse initially broadens due to dispersion, then narrows at increased pulse energies due to stronger SPM.

photonics⁴⁶ are focusing on size and the power budget as essential properties, as well as speed. Research into compact sources with these characteristics is well under way. Laser diodes offer a possible route towards the integration of subpicosecond optical sources. Recent advances in monolithic mode-locking based on quantum dots have pushed pulse widths to below 1 ps (refs 14, 47 and 48), sometimes at the expense of the repetition rate and time–bandwidth product, based on the trade-off optimization of the absorber/gain sections for each cavity length. In parallel to the development of these novel chip-scale light sources, fundamental investigations of soliton-effect pulse compression in PhCWGs, such as in this work, can be cascaded with laser diodes, further compressing pulses deeper into the ultrafast regime in an integrated fashion.

Conclusion

We have demonstrated pulse compression based on high-order solitons at moderately slow group velocities in GaInP PhCWGs. This is enabled by the enhanced SPM and strong negative GVD in the PhCWGs. Use of a material free of two-photon absorption dramatically reduces the impact of nonlinear absorption and free-carrier dispersion, thus preventing detrimental interference with the soliton dynamics. The soliton dynamics emerge from temporal and spectral measurements and are further reinforced with a nonlinear Schrödinger equation model, leading to quantitative agreement with experiments. Owing to the small size of the device (1.3 mm) and low energies (~ 20 pJ), these results are promising developments in the integration of femtosecond and soliton applications in photonic chips.

Methods

Device and linear characterization. The PhC was designed and fabricated as a hexagonal lattice ($p6m$ symmetry group) of air holes arranged in a GaInP slab membrane ($n_0 = 3.13$). Fabrication of a high-quality PhC based on III–V material has achieved record quality factors ($Q > 1 \times 10^6$) in III–V based PhC cavities^{42,49}. Total insertion loss (before and after coupling optics) was estimated to be 8 dB, including 4 dB directly attributable to the coupling optics. Carefully designed integrated mode adapters reduced waveguide coupling losses and suppressed Fabry–Pérot oscillations from facet reflections³⁶. The 3-dB optical transmission band (Supplementary Fig. S1) extended between 1,530 nm and 1,560 nm, and was bounded by the onset of the higher-order odd-mode and the even-mode waveguide cut off. The waveguide dispersion was analysed using the phase-shift method, by measuring the radiofrequency phase modulation of the optical carrier while sweeping the optical frequency through the waveguide transmission³⁹. The measured phase shift $\Delta\phi$ was translated into a time delay through the relationship $\Delta T = \Delta\phi/2\pi f$, where f is the optical carrier frequency and ΔT the propagation delay. The group index is thus

$n_g = c\Delta T/L$. The GVD (β_2) and TOD (β_3) coefficients were obtained from fitting function numerical derivatives.

Experimental pulse characterization. For the pulse compression experiments we used a mode-locked fibre laser (Keopsys/Pritel) delivering nearly transform-limited 2.5–4 ps pulses at a repetition rate of 22 MHz. The source was tunable from 1,525 to 1,565 nm. After adjusting the source to the desired wavelength, we measured the pulse duration and minimized the time–bandwidth product to approach the Fourier limit of hyperbolic secant pulses ($\Delta\lambda\Delta\nu = 0.315$) within 5% (that is, the chirp was negligible). The pulse power was modulated with a variable fibre attenuator, thereby preventing misalignment and undesirable modification of the pulse shape. The second series of experiments was performed using an ~ 100 fs mode-locked fibre laser (Optisiv) operating at 36.5 MHz with a customized picosecond module including a 1.2-nm-wide (FWHM) tunable filter. This generated pulses that were asymmetric in time, with fast rise time and slow fall time, and a total width of ~ 1.8 ps (assuming the deconvolution factor to be equal to 2 for an exponential pulse $\exp(-t/t_0)$ with $t > 0$) and spectral width set by the filter. Autocorrelation traces were recorded using a PulseCheck APE autocorrelator directly coupled to the output of the waveguide. Importantly, we did not use any amplification so as to prevent artefacts and pulse distortion. Owing to the excellent mechanical stability of the set-up and the very good stability of the mode-locked laser, we averaged over 256 autocorrelation traces, thereby improving signal-to-noise ratio. To accommodate the significant change in pulse duration, we collected data with different measurement time spans (5, 15 and 50 ps).

Received 6 July 2010; accepted 6 October 2010;
published online 21 November 2010

References

- Zabusky, N. J. & Kruskal, M. D. Interaction of 'solitons' in a collisionless plasma and the recurrence of initial states. *Phys. Rev. Lett.* **15**, 240–243 (1965).
- Hasegawa, A. & Tappert, F. Transmission of stationary nonlinear optical pulses in dispersive dielectric fibers. I. Anomalous dispersion. *Appl. Phys. Lett.* **23**, 142–144 (1973).
- Mollenauer, L. F., Stolen, R. H. & Gordon, J. P. Experimental observation of picosecond pulse narrowing and solitons in optical fibers. *Phys. Rev. Lett.* **45**, 1095–1098 (1980).
- Eggleton, B. J., Slusher, R. E., de Sterke, C. M., Krug, P. A. & Sipe, J. E. Bragg grating solitons. *Phys. Rev. Lett.* **76**, 1627–1630 (1996).
- Ouzounov, D. G. *et al.* Generation of megawatt optical solitons in hollow-core photonic band-gap fibers. *Science* **301**, 1702–1704 (2003).
- Gerôme, F., Cook, K., George, A., Wadsworth, W. & Knight, J. Delivery of sub-100fs pulses through 8 m of hollow-core fiber using soliton compression. *Opt. Express* **15**, 7126–7131 (2007).
- Dudley, J. M. & Taylor, J. R. Ten years of nonlinear optics in photonic crystal fibre. *Nature Photon.* **3**, 85–90 (2009).
- Foster, M., Gaeta, A., Cao, Q. & Trebino, R. Soliton-effect compression of supercontinuum to few-cycle durations in photonic nanowires. *Opt. Express* **13**, 6848–6855 (2005).

9. Amorim, A. A. *et al.* Sub-two-cycle pulses by soliton self-compression in highly nonlinear photonic crystal fibers. *Opt. Lett.* **34**, 3851–3853 (2009).
10. Zhang, J. *et al.* Optical solitons in a silicon waveguide. *Opt. Express* **15**, 7682–7688 (2007).
11. Dadap, J. I. *et al.* Nonlinear-optical phase modification in dispersion-engineered Si photonic wires. *Opt. Express* **16**, 1280–1299 (2008).
12. Ding, W. *et al.* Solitons and spectral broadening in long silicon-on-insulator photonic wires. *Opt. Express* **16**, 3310–3319 (2008).
13. Nakazawa, M., Kimura, Y., Kurokawa, K. & Suzuki, K. Self-induced-transparency solitons in an erbium-doped fiber waveguide. *Phys. Rev. A* **45**, R23–R26 (1992).
14. Merghem, K. *et al.* Short pulse generation using a passively mode locked single InGaAsP/InP quantum well laser. *Opt. Express* **16**, 10675–10683 (2008).
15. Winful, H. Pulse compression in optical fiber filters. *Appl. Phys. Lett.* **46**, 527–529 (1985).
16. Slusher, R. E. & Eggleton, B. J. (eds) *Nonlinear Photonic Crystals* (Springer Verlag, 2003).
17. Kivshar, Y. S. & Agrawal, G. P. *Optical Solitons: From Fibers to Photonic Crystals* (Academic Press, 2003).
18. Millar, P. *et al.* Nonlinear propagation effects in an AlGaAs Bragg grating filter. *Opt. Lett.* **24**, 685–687 (1999).
19. Baba, T. Slow light in photonic crystals. *Nature Photon.* **2**, 465–473 (2008).
20. Monat, C. *et al.* Slow light enhancement of nonlinear effects in silicon engineered photonic crystal waveguides. *Opt. Express* **17**, 2944–2953 (2009).
21. Soljačić, M. & Joannopoulos, J. D. Enhancement of nonlinear effects using photonic crystals. *Nature Mater.* **3**, 211–219 (2004).
22. McMillan, J. F., Yu, M., Kwong, D.-L. & Wong, C. W. Observation of spontaneous Raman scattering in silicon slow-light photonic crystal waveguides. *Appl. Phys. Lett.* **93**, 251105 (2008).
23. Husko, C. *et al.* Non-trivial scaling of self-phase modulation and three-photon absorption in III-V photonic crystal waveguides. *Opt. Express* **17**, 22442–22451 (2009).
24. Inoue, K., Oda, H., Ikeda, N. & Asakawa, K. Enhanced third-order nonlinear effects in slow-light photonic-crystal slab waveguides of line-defect. *Opt. Express* **17**, 7206–7216 (2009).
25. Yeom, D. I. *et al.* Low-threshold supercontinuum generation in highly nonlinear chalcogenide nanowires. *Opt. Lett.* **33**, 660–662 (2008).
26. Lamont, M. R., Luther-Davies, B., Choi, D. Y., Madden, S. & Eggleton, B. J. Supercontinuum generation in dispersion engineered highly nonlinear ($\gamma = 10/W/m$) As₂S₃ chalcogenide planar waveguide. *Opt. Express* **16**, 14938–14944 (2008).
27. Grillet, C. *et al.* Efficient coupling to chalcogenide glass photonic crystal waveguides via silica optical fiber nanowires. *Opt. Express* **14**, 1070–1078 (2006).
28. Suzuki, K., Hamachi, Y. & Baba, T. Fabrication and characterization of chalcogenide glass photonic crystal waveguides. *Opt. Express* **17**, 22393–22400 (2009).
29. Liao, M. *et al.* Tellurite microstructure fibers with small hexagonal core for supercontinuum generation. *Opt. Express* **17**, 12174–12182 (2009).
30. Peccianti, M. *et al.* Subpicosecond optical pulse compression via an integrated nonlinear chirper. *Opt. Express* **18**, 7625–7633 (2010).
31. Chen, W. & Mills, D. L. Gap solitons and the nonlinear optical response of superlattices. *Phys. Rev. Lett.* **58**, 160–163 (1987).
32. Aceves, A. B. & Wabnitz, S. Self-induced transparency solitons in nonlinear refractive periodic media. *Phys. Lett. A* **141**, 37–42 (1989).
33. Christodoulides, D. N. & Joseph, R. I. Slow Bragg solitons in nonlinear periodic structures. *Phys. Rev. Lett.* **62**, 1746–1749 (1989).
34. Sipe, J. E. & Winful, H. G. Nonlinear Schrödinger solitons in a periodic structure. *Opt. Lett.* **13**, 132–133 (1988).
35. Notomi, M. *et al.* Extremely large group-velocity dispersion of line-defect waveguides in photonic crystal slabs. *Phys. Rev. Lett.* **87**, 253902 (2001).
36. Tran, Q. V., Combrié, S., Colman, P. & De Rossi, A. Photonic crystal membrane waveguides with low insertion losses. *Appl. Phys. Lett.* **95**, 061105 (2009).
37. Engelen, R. J. P., Mori, D., Baba, T. & Kuipers, L. Two regimes of slow-light losses revealed by adiabatic reduction of group velocity. *Phys. Rev. Lett.* **101**, 103901 (2008).
38. Hughes, S., Ramunno, L., Young, J. F. & Sipe, J. E. Extrinsic optical scattering loss in photonic crystal waveguides: role of fabrication disorder and photon group velocity. *Phys. Rev. Lett.* **94**, 033903 (2005).
39. Agrawal, G. P. *Nonlinear Fiber Optics* (Academic Press, 2007).
40. Bhat, N. A. R. & Sipe, J. E. Optical pulse propagation in nonlinear photonic crystals. *Phys. Rev. E* **64**, 056604 (2001).
41. Patterson, M. *et al.* Disorder-induced coherent scattering in slow-light photonic crystal waveguides. *Phys. Rev. Lett.* **102**, 253903 (2009).
42. Combrié, S., Tran, Q., De Rossi, A., Husko, C. & Colman, P. High quality GalnP nonlinear photonic crystals with minimized nonlinear absorption. *Appl. Phys. Lett.* **95**, 221108 (2009).
43. Mollenauer, L. F., Stolen, R. H., Gordon, J. P. & Tomlinson, W. J. Extreme picosecond pulse narrowing by means of soliton effect in single-mode optical fibers. *Opt. Lett.* **8**, 289–291 (1983).
44. De Rossi, A., Conti, C. & Trillo, S. Stability, multistability, and wobbling of optical gap solitons. *Phys. Rev. Lett.* **81**, 85–88 (1998).
45. Claps, R., Dimitropoulos, D., Han, Y. & Jalali, B. Observation of Raman emission in silicon waveguides at 1.54 μm . *Opt. Express* **10**, 1305–1313 (2002).
46. Beausoleil, R. G., Kuekes, P. J., Snider, G. S., Wang, S. Y. & Williams, R. S. Nanoelectronic and nanophotonic interconnects. *Proc. IEEE* **96**, 230–247 (2008).
47. Rafailov, E. U., Cataluna, M. A. & Sibbett, W. Mode-locked quantum-dot lasers. *Nature Photon.* **1**, 395–401 (2007).
48. Kuntz, M., Fiol, G., Laemmlin, M., Meuer, C. & Bimberg, D. High-speed mode-locked quantum-dot lasers and optical amplifiers. *Proc. IEEE* **95**, 1767–1778 (2007).
49. Combrié, S., De Rossi, A., Tran, Q. V. & Benisty, H. GaAs photonic crystal cavity with ultrahigh Q: microwatt nonlinearity at 1.55 μm . *Opt. Lett.* **33**, 1908–1910 (2008).
50. Combrié, S. *et al.* Time-delay measurement in singlemode, low-loss photonic crystal waveguides. *Electron. Lett.* **42**, 86–88 (2006).

Acknowledgements

This work was supported in part by the European Commission GOSPEL project (219299) and the French Research Agency project L2CP (S.C., P.C. and A.D.R.), the National Science Foundation CAREER Award (0747787) and ECCS (0725707) (C.A.H. and C.W.W.), the Fulbright Foundation (C.A.H.), and the New York State Foundation for Science, Technology and Innovation (C.W.W.). The authors acknowledge valuable discussions with E. Ippen, F. Kaertner, G. Eisenstein and S. Trillo. The authors thank Q.-V. Tran for his contributions to the development of the PhC technology in Thales, O. Parillaud, A. Shen and F. Van Dijk (Alcatel-Thales III-V Lab), K. Lasri and U. Ben Ami (Optisiv), and F. Raineri and R. Raj (CNRS-LPN).

Author contributions

P.C., S.C., A.D.R. and C.H. performed the experiments. S.C. and I.S. fabricated the photonic chips, which were designed by S.C. and P.C. A.D.R., P.C. and C.H. performed the modelling. C.H., A.D.R. and C.W.W. prepared the manuscript. A.D.R., I.S. and C.W.W. supervised the project.

Additional information

The authors declare no competing financial interests. Supplementary information accompanies this paper at www.nature.com/naturephotonics. Reprints and permission information is available online at <http://npg.nature.com/reprintsandpermissions/>. Correspondence and requests for materials should be addressed to C.W.W. and A.D.R.